A Flexure-Guided Piezo Drill for Penetrating the Zona Pellucida of Mammalian Oocytes

Wesley Johnson, Changsheng Dai, Jun Liu, Xian Wang, Devin K. Luu, Zhuoran Zhang, Changhai Ru, Chao Zhou, Min Tan, Huayan Pu, Shaorong Xie, Yan Peng, Jun Luo, and Yu Sun

***Abstract*—Mammalian oocytes such as mouse oocytes have a highly elastic outer membrane, zona pellucida (ZP) that cannot be penetrated without significantly deforming the oocyte, even with a sharp micropipette. Piezo drill devices leverage lateral and axial vibration of the micropipette to accomplish ZP penetration with greatly reduced oocyte deformation. However, existing piezo drills all rely on a large lateral micropipette vibration amplitude (>20 μm) and a small axial vibration amplitude (<0.1 μm). The very large lateral vibration amplitude has been deemed to be necessary for ZP penetration although it also induces larger oocyte deformation and more oocyte damage. This paper reports on a new piezo drill device that uses a flexure guidance mechanism and a systematically designed pulse train with an appropriate base frequency. Both simulation and experimental results demonstrate that a small lateral vibration amplitude (e.g., 2 μm) and an axial vibration amplitude as large as 1.2 μm were achieved. Besides achieving 100% effectiveness in the penetration of mouse oocytes ($n = 45$), the new piezo device during ZP penetration induced a small oocyte deformation of 3.4 μm versus larger than 10 μm using existing piezo drill devices.**

***Index Terms*—Cell manipulation, piezo drill, zona pellucida penetration.**

Manuscript received March 22, 2017; revised May 19, 2017; accepted May 29, 2017. Date of publication June 7, 2017; date of current version February 16, 2018. This work was supported in part by the Natural Sciences and Engineering Research Council of Canada, the Canada Research Chairs Program, and the Ontario Research Fund—Research Excellence; in part by the National Natural Science Foundation of China under Grant 61528304, Grant 61525305, and Grant 61403245; and in part by the Shanghai Municipal Science and Technology Commission Project 14JC1491500. *(Wesley Johnson and Changsheng Dai contributed equally to this work.) (Corresponding author: Yu Sun.)*

W. Johnson, C. Dai, J. Liu, X. Wang, D. K. Luu, and Z. Zhang are with the Department of Mechanical and Industrial Engineering, University of Toronto.

C. Ru is with the Jiangsu Provincial Key Laboratory of Advanced Robotics and Collaborative Innovation Center of Suzhou Nano Science and Technology, Soochow University.

C. Zhou and M. Tan are with the Institute of Automation, Chinese Academy of Sciences.

H. Pu, S. Xie, Y. Peng, and J. Luo are with the School of Mechatronic Engineering and Automation, Shanghai University.

Y. Sun is with the Department of Mechanical and Industrial Engineering, University of Toronto, Toronto, ON M5S 3G8, Canada, and also with the School of Mechatronic Engineering and Automation, Shanghai University, Shanghai 200072, China (e-mail: sun@mie.utoronto.ca).

This paper has supplementary downloadable material available at http://ieeexplore.ieee.org (File size: 1.45 MB).

Digital Object Identifier 10.1109/TBME.2017.2713302

I. Introduction

PENETRATING the zona pellucida (ZP) of mammalian oocytes and embryos is an important step in cell surgeries, such as intracytoplasmic sperm injection (ICSI) [1], [2] and biopsy for preimplantation genetic screening (PGS) [3]–[5], for in vitro fertilization, husbandry, and biology research [6], [7]. The ZP is a thick, highly elastic layer composed of glycoproteins surrounding an oocyte or embryo [8] (Fig. 1). Severely deforming the oocyte is typically required for ZP penetration even when a sharp micropipette tip is used [9]. Large oocyte deformation can damage oocyte spindles and lead to failure of oocyte fertilization and embryo development [10].

The use of piezo actuated vibrations can reduce oocyte deformation and improve ZP penetration [11]–[14]. Piezo drills are inertial impact devices [15] using piezoelectric actuators to generate high frequency axial vibrations of a micropipette to induce local rupture of the ZP. Current piezo drill designs cause cell damage by undesired large lateral vibrations on the micropipette tip [Fig. 1(a)]. To help dampen lateral vibrations, a segment of mercury is often used close to the tip of the micropipette [16]. The use of mercury in direct contact with biomaterials causes concerns in clinical practice as well as in biology research. Even with mercury damping, existing piezo drills have a lateral vibration amplitude larger than 20 μm. It has been deemed that such large lateral vibration amplitudes are required for accomplishing ZP penetration [17]–[19].

Fig. 2(a) and (b) summarize existing piezo drill designs. The design shown in Fig. 2(a) has the piezo actuator located far from the micropipette and produces large lateral vibrations on the micropipette tip. Placing the piezo actuator directly behind the micropipette holder can help better focus the vibration at the micropipette tip, as shown in Fig. 2(b). It was reported that this design configuration reduced the lateral vibration to around 20 μm [20], [21] as opposed to over 100 μm in the design shown in Fig. 2(a) [22], when mercury is not used for damping.

This paper presents a new piezo drill design which is capable of generating a substantially larger axial vibration amplitude (1.2 μm vs. <0.1 μm in literature) while significantly reducing the lateral vibration amplitude compared to existing piezo drill designs (<2 μm vs. >20 μm). We further demonstrate that this new piezo drill device is effective in ZP penetration without the need of using mercury for damping. The ZP of mouse oocytes are known for being the most difficult to penetrate among mammalian oocytes because of their significantly higher elasticity

0018-9294 © 2017 IEEE. Personal use is permitted, but republication/redistribution requires IEEE permission.
See http://www.ieee.org/publications_standards/publications/rights/index.html for more information.

Authorized licensed use limited to: CITY UNIV OF HONG KONG. Downloaded on February 14,2025 at 08:33:45 UTC from IEEE Xplore. Restrictions apply.

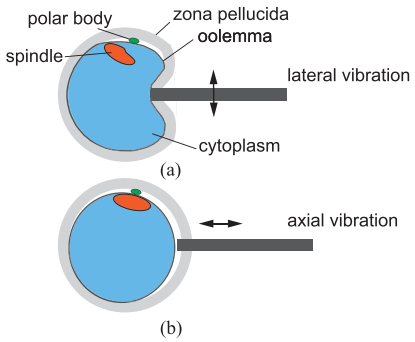

Fig. 1. (a) Present piezo drill devices produce large lateral vibration for penetrating the zona pellucida (ZP) of an oocyte. The resulting oocyte deformation is still relatively large, although not so severe as in passive penetration without using a piezo drill. Large oocyte deformation can cause oocyte spindle dislocation and potential damage. (b) Our new piezo drill is capable of generating a strong axial vibration amplitude while greatly reducing the lateral vibration amplitude to effectively penetrate the ZP with significantly smaller oocyte deformation.

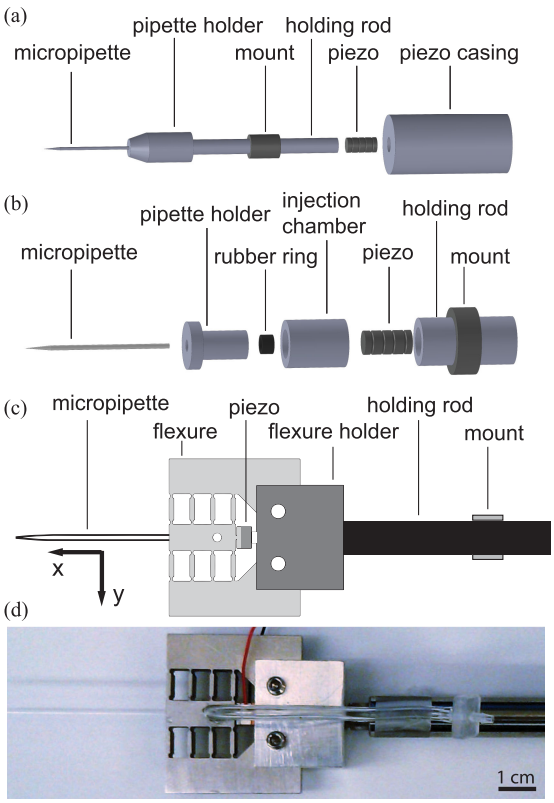

Fig. 2. (a) Design configuration used by PrimeTech and Burleigh in commercial piezo drills [16]. The piezo is located far away from the micropipette resulting in poor control over the actuation direction. (b) Design with the piezo actuator located directly behind the micropipette [20], [25]. (c) Schematic of our design with a flexure guidance structure for controlling actuation direction and dynamics. (d) Picture of our new piezo drill device.

[23]. We used mouse oocytes in experiments to validate the new piezo drill and determine appropriate operational parameters. The results demonstrate that our new piezo drill device is capable of producing a small oocyte deformation of 3.4 μm (vs. >10 μm using existing designs without using mercury for damping) [24].

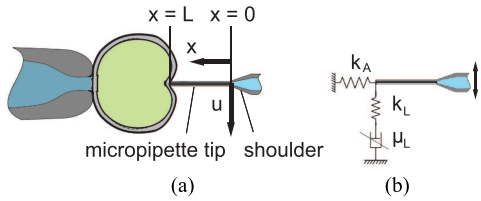

Fig. 3. (a) Micropipette in contact with the ZP. (b) Dynamic model of the micropipette interaction with the ZP.

II. Device Design

For a piezo drill device to achieve a large axial vibration amplitude with suppressed lateral vibration, the device must guide the trajectory of the micropipette in the actuation direction (i.e. axial direction), and the resonant frequencies that result in large lateral vibration must be removed from the input pulse train. By systematic analysis of mode shapes, the piezo drill device, when operated with a carefully selected and filtered pulse train signal, can achieve a large axial vibration amplitude, a low lateral vibration amplitude, and a low oocyte deformation during ZP penetration.

A. Structural Design

As shown in Fig. 2(c) and (d), the flexure-guided design has a piezoelectric actuator integrated on the flexure base. The motion of the micropipette is guided by a number of compliant flexures. The device was manufactured from a single piece of stainless steel by wire electrical discharge machining (EDM); thus, its monolithic structure does not suffer from nonlinearities caused by friction, wear and backlash.

Control over the actuation direction depends on the stiffness ratios between the lateral axes (Y and Z) and the axial axis (X). By achieving a low X-axis stiffness with respect to the other two axes, the motion of the micropipette can be guided in the axial direction irrespective of slight misalignment during device assembly.

B. Micropipette Dynamics

A dynamic model of the micropipette was first established. The objective was to ensure that the micropipette's lateral resonant frequencies are avoided in the design of flexures and the operational pulse train. Fig. 3(a) shows a schematic of the micropipette in contact with an oocyte, and Fig. 3(b) shows the equivalent mechanical system as described in [26].

Using Euler-Bernoulli beam theory, the micropipette tip's equation of motion can be written as

$$EI\frac{\partial^4 u}{\partial x^4} + T\frac{\partial^2 u}{\partial x^2} + \rho A\frac{\partial^2 u}{\partial t^2} + c\frac{\partial u}{\partial t} = 0 \qquad (1)$$

Boundary conditions are

$$u(0,t) = 0, \frac{\partial u(0,t)}{\partial x} = 0, \frac{\partial^2 u(L,t)}{\partial x^2} = 0, \frac{\partial^3 u(L,t)}{\partial x^3} = 0 \quad (2)$$

where u is the lateral displacement of the micropipette tip; x is the position along the micropipette tip before the shoulder; E is the elastic modulus of the micropipette; I is the area moment

Authorized licensed use limited to: CITY UNIV OF HONG KONG. Downloaded on February 14,2025 at 08:33:45 UTC from IEEE Xplore. Restrictions apply.

TABLE I
MICROPIPETTE LATERAL RESONANT FREQUENCIES

Mode		1	2	3	4	5
Frequency (kHz)	Analytical	4.26	26.73	74.85	146.67	242.44
	Numerical	4.26	26.72	74.79	146.43	241.81

of inertia of the micropipette; T is the axial force seen by the micropipette when in contact with the oocyte; ρ and A are the density and sectional area of the micropipette, respectively, used to calculate the mass per unit length; c is the viscous damping coefficient; and L is the length of the micropipette tip.

Assuming the micropipette is in free vibration and harmonic motion, (1) is simplified as

$$EI\frac{\partial^4 u}{\partial x^4} - \rho A\omega^2 u = 0 \tag{3}$$

where ω is the vibration frequency of the micropipette. Rewriting (3) gives

$$\frac{\partial^4 u}{\partial x^4} - \beta^4 u = 0 \tag{4}$$

where $\beta^4 = \frac{\rho A\omega^2}{EI}$, from which resonant frequencies ω_n can be expressed as

$$\omega_n = (\beta_n L)^2\sqrt{\frac{EI}{\rho AL^4}} = k_n^2\sqrt{\frac{EI}{\rho AL^4}} \tag{5}$$

where k_n is the wave number.

The general solution of (3) is

$$u = A\cosh\beta x + B\sinh\beta x + C\cos\beta x + D\sin\beta x \tag{6}$$

Substituting boundary conditions into (6), the characteristic equation is obtained as

$$1 + \cos(\beta_n L)\cosh(\beta_n L) = 1 + \cos k_n \cosh k_n = 0 \tag{7}$$

The first five solutions for k_n are 1.875, 4.694, 7.854, 10.996, 14.137. The geometrical parameters of the micropipette include $L = 1.5$ mm, outer diameter $D_o = 10$ μm, inner diameter $D_i = 8\,\mu$m, $A = 2.83 \times 10^{-11}$ m^2, and $I = \frac{\pi}{64}(D_o^4 - D_i^4) = 2.90 \times 10^{-22}$ m^4. The material properties are $\rho = 2{,}230$ kg/m^3 and $E = 64$ GPa for borosilicate glass.

By substituting micropipette parameters and wave number k_n into (5), we analytically solved the first five resonant frequencies. Finite element analysis of the micropipette was also performed to obtain the numerical solutions of resonant frequencies. The analytical and numerical results are in consistent agreement as summarized in Table I. The finite element model was later used to simulate the vibration of the micropipette.

When the piezo drill is operated at a frequency sufficiently far from the micropipette's lateral resonant frequencies, the micropipette's motion can stay largely along the axial direction. Therefore, the operation frequency ranges of 0–3 kHz and 7–20 kHz were targeted for inducing low lateral vibrations.

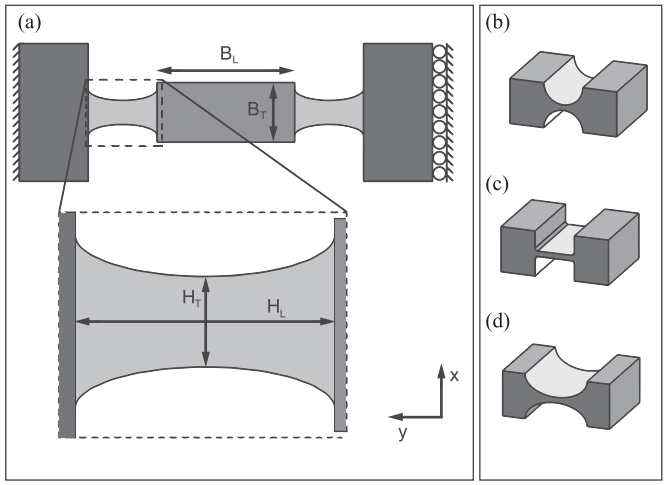

Fig. 4. (a) Flexure configuration chosen in the design of our piezo drill device. The parameters that need to be determined are labelled. (b)–(d) Three different hinge configurations: (b) circular, (c) corner-filleted, and (d) elliptical.

C. Flexure Dynamics

The piezo drill uses a flexure guidance mechanism. Flexure mechanism uses the elastic deformation of the material to deliver motion, and is widely used in precision positioning applications [27], [28]. For flexure design, the inner section of a uniform beam is thickened to strengthen its out-of-plane (Z) stiffness [29], [30], which results in the double hinged beam configuration shown in Fig. 4(a). Fig. 4(b)–(d) show candidate geometries for the hinges. Circular hinges [Fig. 4(b)] have a high out-of-plane stiffness but a low motion range. Corner filleted hinges [Fig. 4(c)] have a large motion range but a poor out-of-plane stiffness. Elliptical hinges [Fig. 4(d)] combine these properties allowing for a stiff flexure while maintaining a relatively low stress at maximum extension for the flexure to have a long fatigue life [31], [32]. For the chosen flexure configuration shown in Fig. 4(a), the six parameters of the flexure that need to be determined are the number of beams, beam thickness (B_T), beam length (B_L), hinge shape, hinge pivot point thickness (H_T), and hinge length (H_L).

Stainless steel was chosen to construct the piezo drill device because of its high yield strength (505 MPa), which is significantly higher than the predicted maximum stress of 250 MPa encountered during vibration.

The selected piezoelectric actuator (TA0505D024W, Thorlabs Inc.) is compact (5 mm $\times$ 5 mm $\times$ 2.4 mm) and has a displacement output up to 2.8 μm $\pm$ 15%. Considering that the blocking force of this piezo actuator is 400 N and typically a piezo is preloaded with one quarter of its blocking force, a 100 N preload was used in our design [33]. Preload was implemented by pressing the piezoelectric actuator against the flexure with a screw and a metal shim. The 100 N preloading force was calibrated by measuring the screw torque with a vertical torque gauge (S0-12, Seekonk). The axial force exerted by the screw was calculated with the measured torque, screw diameter, and friction coefficient. Sufficiently preloading the piezo is

Authorized licensed use limited to: CITY UNIV OF HONG KONG. Downloaded on February 14,2025 at 08:33:45 UTC from IEEE Xplore. Restrictions apply.

TABLE II
DIMENSIONS OF FLEXURE ELEMENTS FROM SIMULATION

B_L (mm)	B_T (mm)	B_W (mm)	H_L (mm)	H_T (mm)	Flexure Number
7	1.2	5	1	0.3	8

TABLE III
SYSTEM VALUES DETERMINED BY FINITE ELEMENT STRUCTURAL SIMULATION

k_x (N/μm)	k_y (N/μm)	k_z (N/μm)	X-axis resonant frequency (Hz)	max stress at 100 N (MPa)
3.5	230.5	200.1	24,927	250

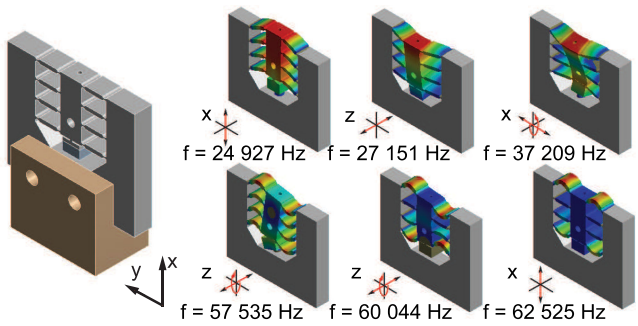

Fig. 5. Modal analysis showing the mode shapes, translational resonant frequencies, and rotational resonant frequencies.

important for ensuring its stability and avoiding brittle fracture at operating frequencies approaching or above the flexure's resonant frequencies.

The X-axis resonant frequency must be higher than the input pulse's frequency to avoid initiating flexure or micropipette resonance. However, too high an X-axis resonant frequency requires a high stiffness k_x. Low stiffness ratios, k_y/k_x and k_z/k_x can cause large off-axis motion and large lateral vibration. Considering the selected frequency ranges of 0–3 kHz and 7–20 kHz (see Section II-B), the X-axis resonant frequency of 25 kHz was chosen in the design.

With the target X-axis resonant frequency of 25 kHz and a preload of 100 N, iterative finite element structural simulation was conducted. Tables II and III summarize the determined flexure dimensions and other major parameters. The complete piezo drill device has a footprint of 40 mm $\times$ 36 mm $\times$ 15 mm.

Modal analysis was then performed. As shown in Fig. 5, X-axis resonance occurs at approximately 25 kHz which is lower than all other translational and rational resonant frequencies. The X-axis resonant frequency must be lower than all other resonant frequencies to achieve strong axial vibrations.

D. Driving Pulse Train Design

As discussed in Section II-B, operating the device at a continuous frequency in the ranges of 0–3 kHz and 7–20 kHz can result in low lateral vibrations. Piezo drills use a pulse train to penetrate the ZP of an oocyte with reduced energy transfer for less oocyte damage [22]. A driving pulse train is formed by applying multiple pulses per second with intervals among them; thus, it contains less energy compared to continuous driving signals. A continuous sinusoidal signal has all of its spectral power at one point [see Fig. 6(a) and (b), frequency: 18 kHz]. Fig. 6(c) shows a pulse with a base frequency of 18 kHz generated from the continuous sinusoidal signal shown in Fig. 6(a). Its frequency response [Fig. 6(d)] contains values from all frequencies including 3–7 kHz and above 20 kHz which can cause lateral resonance.

A band-stop filter with cutoff frequencies of [3 kHz, 7 kHz] and a low-pass filter with a cutoff frequency of 20 kHz were used to filter the original pulse signal shown in Fig. 6(c). Both filters are second-order infinite impulse response (IIR) filters, expressed as

$$y[n] = \sum_{k=0}^{2} b_k x[n-k] - \sum_{k=1}^{2} a_k y[n-k] \tag{8}$$

where y and x are the output and input of the filters, b_k is the kth feed-forward coefficient, and a_k is the kth feedback coefficient. For the low-pass filter, $b_0 = 3 \times 10^{-4}$, $b_1 = 6 \times 10^{-4}$, $b_2 = 3 \times 10^{-4}$, $a_1 = -5.85 \times 10^{-4}$, $a_2 = 2.85 \times 10^{-4}$. For the band-stop filter, $b_0 = 0.99$, $b_1 = -1.98$, $b_2 = 0.99$, $a_1 = -1.97$, $a_2 = 0.98$.

The filtered pulse signal is shown in Fig. 6(e) and (f). It can be seen that this filtered pulse has the undesired frequency ranges of 3–7 kHz and above 20 kHz significantly attenuated.

When the piezo drill device was used in experiments, the filtered pulse shown in Fig. 6(e) was applied multiple times within a second (100 pulses), which forms a pulse train, to the piezo actuator as the driving signal for ZP penetration. The amplitude of the driving pulse can be altered by varying the peak voltage, which was varied from 4 V to 20 V with 4 V increments in the experiments. The speed of the micropipette was approximated as the amplitude of its axial motion divided by the peak time [Fig. 6(e)] of the driving pulse.

III. EXPERIMENTAL RESULTS AND DISCUSSION

A. Vibration Simulation

To validate the piezo drill design and analyze the causes of micropipette tip's lateral vibration, finite element simulation was conducted. Simulation showed that the designed piezo drill produces strong axial vibration and small lateral vibration, and the reduction of the lateral vibration is due to the suppression of flexure off-axis oscillation. In the finite element model [Fig. 7(a)], a driving pulse with the frequency of 18 kHz and peak voltage of 20 V was applied to the piezoelectric actuator. The period of a driving pulse is 56 μs (corresponding to 18 kHz), which is significantly shorter than the 10 ms period of a pulse train (100 pps). Thus, the transient responses of the flexure and the micropipette under a single driving pulse were studied.

With this driving pulse, the actuator outputs a displacement with the amplitude of 0.8 μm, which is exerted at the interface between the flexure and the actuator. In simulation, this displacement of 0.8 μm was assumed to deviate from the axial

Authorized licensed use limited to: CITY UNIV OF HONG KONG. Downloaded on February 14,2025 at 08:33:45 UTC from IEEE Xplore. Restrictions apply.

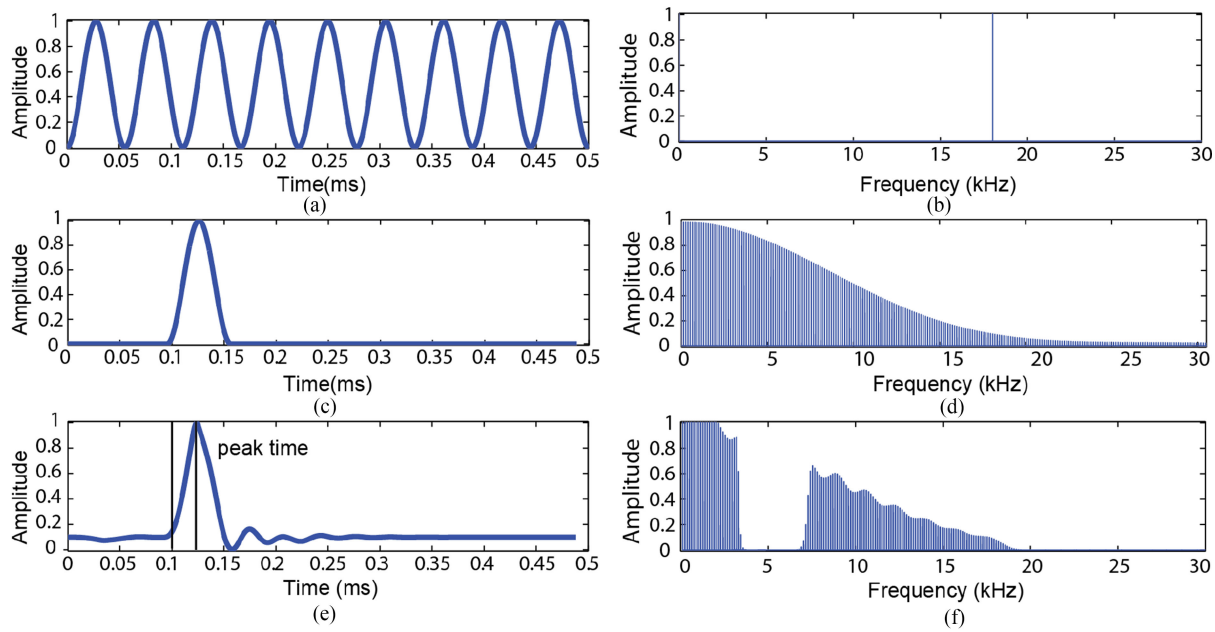

Fig. 6. (a), (b) A sinusoidal signal (frequency: 18 kHz) has a spectral power at one point. (c), (d) A pulse with a base frequency of 18 kHz. The full spectrum shown in the FFT will trigger lateral resonance in the micropipette. (e), (f) The pulse shown in (c) is filtered, and frequencies of 3–7 kHz and above 20 kHz are attenuated.

direction by 6° to take the effect of misalignment in device assembly into account, resulting in a lateral amplitude of 0.08 μm and an axial amplitude of 0.796 μm at the interface between flexure and the actuator [Fig. 7(d)]. These displacement amplitudes are transmitted to the micropipette base where the flexure and micropipette are connected and further to the micropipette tip.

Fig. 7(b) and (c) show the axial and lateral vibrations of the flexure (where flexure and micropipette are connected) and the micropipette tip. The flexure has an axial vibration amplitude of 1.00 μm and a lateral vibration amplitude of 14.27 nm. Transmitted from the piezoelectric actuator through the flexure, the axial vibration amplitude of the micropipette tip is 1.24 μm, and the lateral vibration amplitude is 0.62 μm. Compared to the flexure, the micropipette's axial vibration amplitude is slightly larger than the flexure's axial vibration amplitude (1.24 μm vs. 1.00 μm) [Fig. 7(b)] because the micropipette, made of borosilicate glass and firmly attached to the flexure, experiences elastic deformations along the axial direction due to inertia. For lateral vibration, flexure's vibration amplitude is significantly amplified when transmitted to the micropipette tip [Fig. 7(c)].

The lateral vibration of the micropipette tip stems from both the lateral deflection of the micropipette and the flexure off-axis oscillation [Fig. 7(e)]. When subject to lateral vibration, the micropipette tip undergoes lateral deflection because the micropipette tip is highly flexible as a thin beam with a high length-to-diameter ratio of 150. In the meanwhile, the flexure off-axis oscillation makes the base of the micropipette subject to not only lateral translation but also rotation.

To understand the individual contribution of the micropipette's lateral deflection and the flexure oscillation to the lateral vibration of the micropipette tip, we modeled the micropipette tip as a cantilever [Fig. 7(f)] undergoing only lateral deflection when subject to the lateral displacement of the micropipette after shoulder. Because the segment of micropipette after shoulder (1 mm diameter vs. 10 μm for micropipette tip) is orders of magnitude stiffer than micropipette tip, the lateral displacement input to the micropipette tip was taken from the lateral amplitude of the micropipette base (i.e., where flexure and micropipette are connected), which is 14.27 nm. As shown in Fig. 7(g), the resulting lateral vibration amplitude of the micropipette tip is 110.00 nm, which is the sum of the lateral deflection of the micropipette tip and the lateral displacement of the micropipette after shoulder. This value of 110.00 nm accounts for a very small portion of the overall lateral vibration amplitude of 0.62 μm; therefore, the lateral vibration amplitude of the micropipette tip mostly results from the flexure oscillation. As an example, for a 0.1° flexure oscillation, the lateral vibration amplitude of the 1.5 mm long micropipette tip is as large as $1500\sin(0.1^\circ) = 2.6\,\mu$m. In our design, suppression of flexure oscillation is well accomplished by the high stiffness ratios, k_y/k_x and k_z/k_x (see Table III).

To study the damping effect of liquid when the micropipette tip is immersed into the culture medium during oocyte penetration, simulation of the micropipette tip in liquid was also performed. The results show that in liquid (viscosity $\mu = 1.003\,\text{mPa}\cdot\text{s}$, density $\rho = 998.2\,\text{kg/m}^3$) the micropipette tip has an axial vibration amplitude of 1.21 μm and a lateral vibration amplitude of 0.23 μm, as shown in Fig. 7(b) and (c). The axial vibration amplitude of the micropipette tip only becomes slightly lower (1.21 μm in liquid vs. 1.24 μm in vacuum), but the lateral vibration amplitude is reduced by 63% (0.23 μm in liquid vs. 0.62 μm in vacuum). The results indicate that the piezo drill can maintain strong axial vibration with lateral vibration significantly reduced when the micropipette tip is immersed in liquid.

Authorized licensed use limited to: CITY UNIV OF HONG KONG. Downloaded on February 14,2025 at 08:33:45 UTC from IEEE Xplore. Restrictions apply.

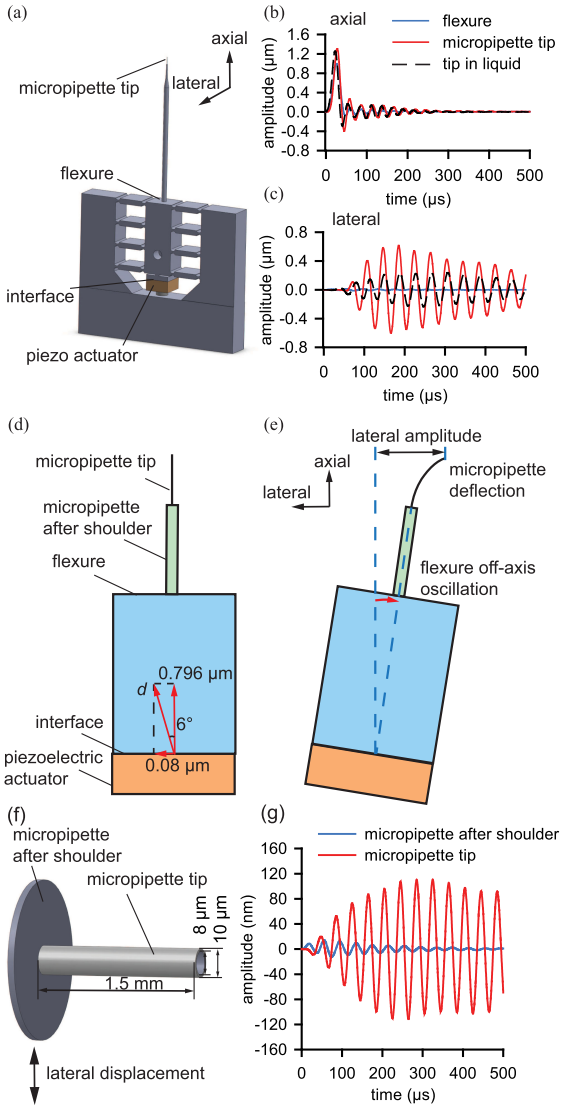

Fig. 7. (a) Simulation model for the designed piezo drill. The output displacement of the piezoelectric actuator is exerted at the interface between the flexure and the actuator. For vibration analysis, locations are 1) where the micropipette and flexure are connected; and 2) the micropipette tip. (b) Axial vibration of the flexure and the micropipette. The vibration amplitude of the micropipette tip is larger than that of the flexure due to the elastic deformation of the micropipette along the axial direction under inertia. (c) Lateral vibration of the flexure and the micropipette. The vibration amplitude is significantly amplified from the flexure to the micropipette tip because of micropipette deflection and flexure oscillation. (d) Diagram of the piezo drill. The displacement $d = 0.8$ μm is exerted at the interface between the piezoelectric actuator and the flexure, and deviates from the axial direction by 6° due to misalignment in device assembly. (e) The lateral vibration amplitude of the micropipette tip is the combination of flexure oscillation and micropipette deflection. (f) Cantilever model of the micropipette tip. The lateral vibration of the micropipette tip is induced by the lateral displacement of the micropipette after shoulder. (g) The lateral vibration of the micropipette tip and the micropipette after shoulder. The lateral vibration of the micropipette tip, in this case, is caused only by the deflection of the micropipette tip.

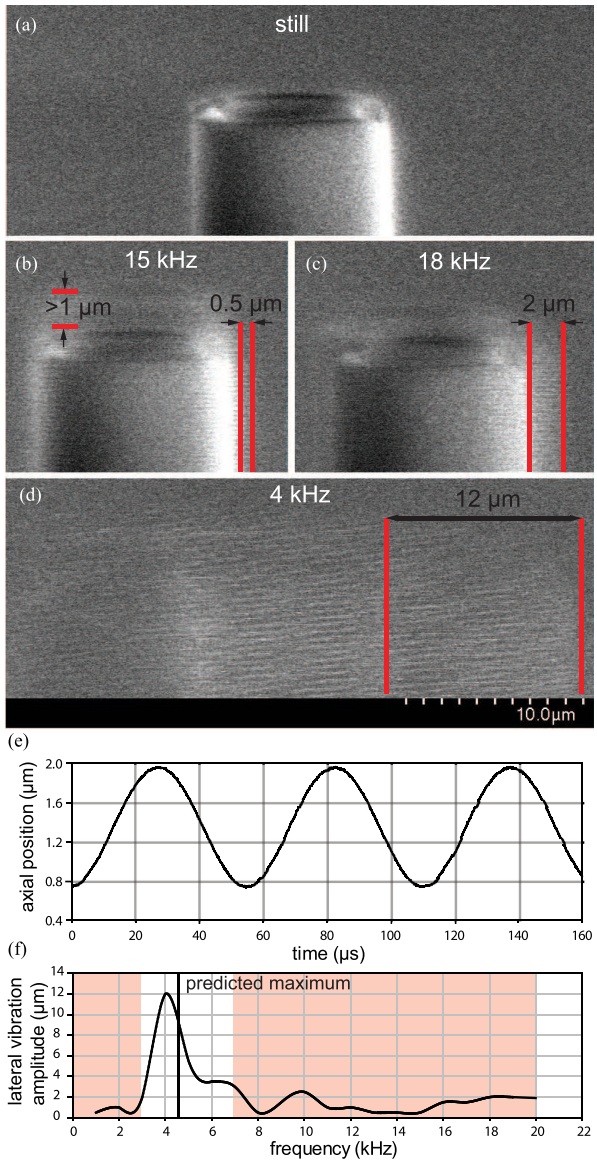

Fig. 8. (a) SEM image of the micropipette tip before a driving pulse was supplied to the piezo actuator. (b) Driving pulses of 15 kHz produced a lateral vibration amplitude of approximately 500 nm and an axial vibration amplitude of approximately 1.2 μm. (c) Driving pulses of 18 kHz produced a lateral vibration amplitude of approximately 2 μm, and the axial vibration amplitude was still approximately 1.2 μm. (d) Driving pulses of 4 kHz produced a large lateral vibration amplitude of 12 μm. (e) Micropipette's axial vibration amplitude measured by laser doppler vibrometry. The frequency of the supplied driving pulses was 18 kHz. (f) Frequency response of the micropipette. The highlighted regions are frequency ranges selected for avoiding the resonance of the micropipette tip.

B. Micropipette's Vibration Behavior

We first used scanning electron microscopy (SEM, SU3500, Hitachi) to characterize the micropipette's vibration amplitudes. SEM imaging has a low bandwidth (20 Hz); thus, as the micropipette vibrates, its vibrational envelope appears in SEM imaging as blurred edges [see Fig. 8(b)–(d)]. Measuring the distance between an edge of the micropipette and its corresponding vibration-caused blurry edge enabled the quantification of the micropipette's axial and lateral vibration amplitudes.

Fig. 8(b)–(d) correspond to 15 kHz, 18 kHz, and 4 kHz, respectively, which are the frequencies of the driving pulse supplied to the piezoelectric actuator. The peak voltage of the driving pulse was held constant at 20 V. It can be seen in Fig. 8(d) that 4 kHz driving pulses produced a large lateral vibration amplitude of 12 μm on the micropipette tip because 4 kHz is close to

Authorized licensed use limited to: CITY UNIV OF HONG KONG. Downloaded on February 14,2025 at 08:33:45 UTC from IEEE Xplore. Restrictions apply.

the first lateral resonant frequency of the micropipette (4.26 kHz, see Table I). When 15 kHz driving pulses [Fig. 8(b)] were applied to the piezo actuator, the micropipette tip had a lateral vibration amplitude of 500 nm and an axial vibration amplitude of 1.2 μm. When the driving pulse's frequency was increased to 18 kHz [Fig. 8(c)], the micropipette's axial vibration amplitude was still approximately 1.2 μm; however, the lateral vibration amplitude increased to 2 μm (vs. 0.5 μm produced by 15 kHz driving pulses).

We then used a laser Doppler vibrometer (OFV-5000, Polytec) to verify the micropipettes axial vibration amplitude measured by SEM. The displacement resolution of the vibrometer is better than 1 nm. With 18 kHz driving pulses, the axial vibration amplitude measured by the laser doppler vibrometer was 1.2 μm [see Fig. 8(e)], in agreement with the SEM measured results. The experimentally measured axial vibration amplitude is consistent with the value predicted in finite element simulation (1.2 μm vs. 1.24 μm); however, the simulation-predicted lateral vibration amplitude is smaller than the experimentally measured value (0.62 μm vs. 2 μm). This discrepancy is likely due to hysteresis and fluctuation in the displacements generated by the piezoelectric actuator. Piezoelectric actuators exhibit hysteresis due to crystalline polarization effects and molecular friction, which can cause considerable nonlinearity in displacement [34], [35].

SEM images were also used to measure the frequency response of the micropipette along the lateral direction. To quantify the lateral vibration amplitudes, the driving pulse's frequency was increased with an increment of 1 kHz each time, and the lateral vibration amplitude was measured from the SEM images. As summarized in Fig. 8(f), it can be seen that in the range of 8–20 kHz for the driving pulse's frequency, the lateral vibration amplitude of the micropipette was consistently within 2 μm. SEM and vibrometry measurements were made in vacuum and in air, respectively. When the micropipette tip operates in liquid, simulation indicated that the lateral vibration amplitude can be reduced by 63% [see Fig. 7(c)]. Therefore, with 18 kHz driving pulses, we can estimate that the lateral vibration amplitude in liquid could be reduced from 2 μm as measured in vacuum (SEM) and in air (vibrometry) to 0.74 μm.

C. Mouse Oocyte ZP Penetration

The zona pellucida (ZP) of mouse oocytes is known to be the most difficult to penetrate among all mammalian oocytes. Thus, we conducted ZP penetration experiments using mouse oocytes for evaluating the performance of our new piezo drill device. Mouse oocytes used in this work were gathered from the Canadian Mouse Mutant Repository in the Toronto Centre for Phenogenomics. The success rate of ZP penetration with the piezo drill was 100% based on the testing of 45 mouse oocytes.

Fig. 9(a) and (b), corresponding to supplied driving pulses of 18 kHz and peak voltage of 20 V, show that the piezo drill was capable of penetrating the ZP of mouse oocytes with small oocyte deformation (see Supplementary Video). As summarized in Fig. 9(c), oocyte deformation decreased when the driving pulse's frequency was increased. At 18 kHz, oocyte deformation was as small as 3.4 $\pm$ 1.7 μm.

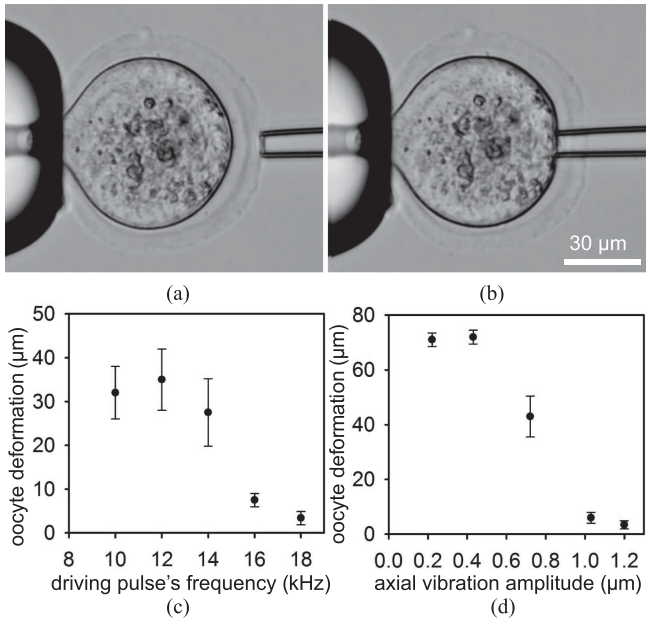

Fig. 9. (a), (b) ZP penetration with little oocyte deformation. Driving pulse's frequency and peak voltage were 18 kHz and 20 V, respectively. (c) Oocyte deformation at penetration vs. driving pulse's frequency. n = 4; total number of oocytes measured: 20. Peak voltage was 20 V. (d) Oocyte deformation at penetration vs. axial vibration amplitude. n = 5; total number of oocytes measured: 25. Driving pulse's frequency was 18 kHz.

TABLE IV
PIEZO DRILL PERFORMANCE AT SELECTED FREQUENCIES

frequency (kHz)	axial vibration amplitude (μm)	lateral vibration amplitude (μm)	micropipette speed (mm/s)	average deformation at penetration (μm)
14	1.2	0.5	33.6	27.5
16	1.2	1.5	38.4	7.5
18	1.2	2	43.2	3.4

Peak voltage of the driving pulse was 20 V in all cases.

Fig. 9(d) shows that oocyte deformation at penetration decreased as the piezo drills axial vibration amplitude increased. In experiments, a higher axial vibration amplitude was achieved by applying a larger peak voltage in the driving pulse. From Table IV, one can also see that when the driving frequency was increased with peak voltage held constant (20 V), the micropipette's motion speed also became higher. At a low motion speed, the micropipette significantly deformed the oocyte. It has been shown that penetrating the ZP at a low speed requires the production of high tensile stress in the ZP until it reaches a critical value for ZP rupturing [9], [36]. With a higher motion speed, this critical tensile stress becomes significantly lower, making ZP penetration easier.

Existing piezo drills all have a large lateral vibration amplitude (>20 μm) and a very low axial vibration amplitude (<0.1 μm). It was deemed that a large lateral vibration

Authorized licensed use limited to: CITY UNIV OF HONG KONG. Downloaded on February 14,2025 at 08:33:45 UTC from IEEE Xplore. Restrictions apply.

amplitude is necessary for ZP penetration. Differently, our results indicate that a large axial vibration amplitude and a small lateral vibration amplitude are highly effective in ZP penetration. For instance, with a driving pulse's frequency of 18 kHz and a peak voltage of 20 V, the axial vibration amplitude was 1.2 μm and the lateral vibration amplitude was 2 μm. Under this condition, the average oocyte deformation was 3.4 μm (Table IV). In comparison, existing piezo drills produce mouse oocyte deformations larger than 10 μm unless a drop of mercury is used in the micropipette for damping.

The data in Table IV also shows that even though the axial vibration amplitude is large, too low a lateral vibration amplitude (e.g. 0.5 μm for 14 kHz) still resulted in a large oocyte deformation with a mean value of 27.5 μm. When the lateral vibration amplitude was increased to 2 μm (see 18 kHz), oocyte deformation became as small as 3.4 μm. Although the micropipette speed also increases when driving pulses frequency rises, speed alone cannot explain significant decrease of oocyte deformation as the increase of the micropipette speed is not comparably significant. The decrease of oocyte deformation should be mainly attributed to the increase of lateral vibration amplitude. The results suggest that lateral vibration is necessary for ZP penetration; however, the lateral vibration amplitude does not need to be higher than 2 μm (vs. $>$20 μm in existing piezo drills) when the axial vibration amplitude is larger than 1 μm (vs. $<$0.1 μm in existing piezo drills). Mouse ZP penetration under these conditions was highly effective (100% successful based on the 45 oocytes tested) with significantly reduced oocyte deformation (3.4 μm vs. 10 μm using existing piezo drills). Further increasing the lateral vibration amplitude from 2 μm to a higher value induced larger oocyte deformation in experiments since large lateral vibration can create more strain on oocyte ZP [17].

Both axial and lateral vibrations play a role in ZP penetration. The axial movement of the micropipette tip introduces tensile stress on ZP and leads to ZP rupture when the exerted tensile stress surpasses the critical tensile stress of ZP. Large axial vibration of the micropipette tip can lower the critical tensile stress by punching the ZP at a high speed [36], making the penetration of ZP easier and oocyte deformation reduced. Lateral vibration of the micropipette tip exerts strain on the zone of contact with ZP. It was reported, via simulating ZP as an elastodamage model, that the strain caused by micropipette's lateral vibration can lead to local failure of ZP, and stress accumulation can occur around the failure site, facilitating ZP rupture [17]. Micropipette's lateral vibration can also locally push ZP away from the zone of contact between the micropipette tip and ZP, reducing the friction between them. Thus, lateral vibration helps maintain the impact energy of axial vibration by lowering friction-caused energy loss. This is analogous to the ultrasonic vibration induced by piezoelectric actuators in the application of ultrasonic cutting where the friction between the cutting tool and the workpiece is reduced [37]. However, lateral vibration should be limited (e.g., 2 μm) in order not to induce large oocyte deformation during ZP penetration for preserving oocyte spindle integrity [10].

IV. Conclusion

This paper presented a new piezo drill device for penetrating the ZP of mouse oocytes. Through systematically performing structure modeling and dynamic analysis, design parameters were rationally chosen. The designed flexure-based piezo drill can guide the motion of the micropipette along the axial direction and reduce lateral vibration. An approach for selecting proper driving pulses was also developed. Finite element models were established to guide the design of the piezo drill, and it was found that reducing flexure off-axis oscillation is critical for suppressing micropipette's lateral vibration. SEM and laser doppler vibrometry measurements quantitatively related driving pulse's frequency and resulting lateral and axial vibration amplitudes. Experiments on mouse oocytes revealed that this piezo drill is capable of generating strong axial vibration and small lateral vibration, which together were proven to be effective for ZP penetration with small oocyte deformation. This is drastically different from the previous belief that a large lateral vibration amplitude is necessary for penetrating the ZP.

References

[1] Z. Lu *et al.*, "Robotic ICSI (intracytoplasmic sperm injection)," *IEEE Trans. Biomed. Eng.*, vol. 58, no. 7, pp. 2102–2108, Jul. 2011.

[2] P. Rubino *et al.*, "The ICSI procedure from past to future: A systematic review of the more controversial aspects," *Human Reprod. Update*, vol. 22, no. 2, pp. 194–227, 2016.

[3] K. Sermon *et al.*, "Preimplantation genetic diagnosis," *Lancet*, vol. 363, no. 9421, pp. 1633–1641, 2004.

[4] S. Mastenbroek and S. Repping, "Preimplantation genetic screening: Back to the future," *Human Reprod.*, vol. 29, no. 9, pp. 1846–1850, 2014.

[5] R. S. Zimmerman *et al.*, "Development and validation of concurrent preimplantation genetic diagnosis for single gene disorders and comprehensive chromosomal aneuploidy screening without whole genome amplification," *Fertility Sterility*, vol. 105, no. 2, pp. 286–294, 2016.

[6] M. Khalilian *et al.*, "Estimating zona pellucida hardness under microinjection to assess oocyte/embryo quality: Analytical and experimental studies," *Adv. Biosci. Biotechnol.*, vol. 4, no. 5, pp. 679–688, 2013.

[7] L. A. Hyslop *et al.*, "Towards clinical application of pronuclear transfer to prevent mitochondrial DNA disease," *Nature*, vol. 534, pp. 383–386, 2016.

[8] L. Andolfi *et al.*, "Investigating the mechanical properties of zona pellucida of whole human oocytes by atomic force spectroscopy," *Integr. Biol.*, vol. 8, no. 8, pp. 886–893, 2016.

[9] Y. Sun *et al.*, "Mechanical property characterization of mouse zona pellucida," *IEEE Trans. Nanobiosci.*, vol. 2, no. 4, pp. 279–286, 2003.

[10] Z. Luo *et al.*, "Deformation of a single mouse oocyte in a constricted microfluidic channel," *Microfluidics Nanofluidics*, vol. 19, no. 4, pp. 883–890, 2015.

[11] Y. Kimura and R. Yanagimachi, "Intracytoplasmic sperm injection in the mouse," *Biol. Reprod.*, vol. 52, no. 4, pp. 709–720, 1995.

[12] S. Takeuchi *et al.*, "Comparison of piezo-assisted micromanipulation with conventional micromanipulation for intracytoplasmic sperm injection into human oocytes," *Gynecologic Obstetric Investigation*, vol. 52, no. 3, pp. 158–162, 2001.

[13] K. Yanagida *et al.*, "The usefulness of a piezo-micromanipulator in intracytoplasmic sperm injection in humans," *Human Reprod.*, vol. 14, no. 2, pp. 448–453, 1999.

[14] H. Katayose *et al.*, "Efficient injection of bull spermatozoa into oocytes using a piezo-driven pipette," *Theriogenology*, vol. 52, no. 7, pp. 1215–1224, 1999.

[15] T. Higuchi *et al.*, "Precise positioning mechanism utilizing rapid deformations of piezoelectric elements," in *Proc. IEEE Workshop Micro Electro Mech. Syst.*, 1990, pp. 222–226.

[16] N. Yoshida and A. C. Perry, "Piezo-actuated mouse intracytoplasmic sperm injection (ICSI)," *Nature Protocols*, vol. 2, no. 2, pp. 296–304, 2007.

Authorized licensed use limited to: CITY UNIV OF HONG KONG. Downloaded on February 14,2025 at 08:33:45 UTC from IEEE Xplore. Restrictions apply.

[17] Y. Gan and Z. Chen, "A study of the zona piercing process in piezodriven intracytoplasmic sperm injection," *J. Appl. Phys.*, vol. 104, no. 4, 2008, Art. no. 044702.
[18] Z. N. Wang *et al.*, "Application of lateral oscillating piezo-driven micropipette in embryo biopsy for pre-implantation genetic diagnosis," in *Proc. IEEE Int. Conf. Control Autom. Robot. Vis.*, 2014, pp. 1218–1223.
[19] Z. Wang *et al.*, "Beneficial micropipette oscillation in vision-guided piezo-assisted ICSI," in *Proc. IEEE Int. Conf. Robot. Biomimetics*, 2013, pp. 1665–1670.
[20] H. B. Huang *et al.*, "Piezoelectric driven non-toxic injector for automated cell manipulation," in *Proc. Med. Meets Virtual Reality Conf.*, 2011, pp. 231–235.
[21] Z. Ge *et al.*, "Optimal design of a new structure piezo-driven cell injector," in *Proc. IEEE Int. Conf. Nanotechnol.*, 2014, pp. 525–530.
[22] K. Ediz and N. Olgac, "Microdynamics of the piezo-driven pipettes in ICSI," *IEEE Trans. Biomed. Eng.*, vol. 51, no. 7, pp. 1262–1268, Jul. 2004.
[23] X. Liu *et al.*, "In situ mechanical characterization of mouse oocytes using a cell holding device," *Lab Chip*, vol. 10, no. 16, pp. 2154–2161, 2010.
[24] P. Pan *et al.*, "An improved technology without mercury for cellular piercing," in *Proc. IEEE Int. Conf. Nanotechnol.*, 2014, pp. 164–167.
[25] H. Huang *et al.*, "A new piezo-driven ultrasonic cell microinjection system," in *Proc. IEEE Int. Conf. Inf. Autom.*, 2010, pp. 18–23.
[26] M. Karzar-Jeddi *et al.*, "Dynamic response of micropipettes during piezo-assisted intracytoplasmic sperm injection," *Phys. Rev. E*, vol. 84, no. 4, 2011, Art. no. 041908.
[27] Q. Xu, "New flexure parallel-kinematic micropositioning system with large workspace," *IEEE Trans. Robot.*, vol. 28, no. 2, pp. 478–491, Apr. 2012.
[28] Q. Xu, "Precision motion control of piezoelectric nanopositioning stage with chattering-free adaptive sliding mode control," *IEEE Trans. Autom. Sci. Eng.*, vol. 14, no. 1, pp. 238–248, Jan. 2017.
[29] Y. Yong *et al.*, "Invited review article: High-speed flexure-guided nanopositioning: Mechanical design and control issues," *Rev. Sci. Instrum.*, vol. 83, no. 12, 2012, Art. no. 121101.
[30] B. J. Kenton and K. K. Leang, "Design and control of a three-axis serial-kinematic high-bandwidth nanopositioner," *IEEE/ASME Trans. Mechatron.*, vol. 17, no. 2, pp. 356–369, Apr. 2012.
[31] B. J. Kenton *et al.*, "Compact ultra-fast vertical nanopositioner for improving scanning probe microscope scan speed," *Rev. Sci. Instrum.*, vol. 82, no. 12, 2011, Art. no. 123703.
[32] K. K. Leang and A. J. Fleming, "High-speed serial-kinematic SPM scanner: Design and drive considerations," *Asian J. Control*, vol. 11, no. 2, pp. 144–153, 2009.
[33] J. Chen and I. Dwang, "A ballscrew drive mechanism with piezo-electric nut for preload and motion control," *Int. J. Mach. Tools Manuf.*, vol. 40, no. 4, pp. 513–526, 2000.
[34] C. Ru *et al.*, "A hysteresis compensation method of piezoelectric actuator: Model, identification and control," *Control Eng. Pract.*, vol. 17, no. 9, pp. 1107–1114, 2009.
[35] Q. Xu, "Digital integral terminal sliding mode predictive control of piezoelectric-driven motion system," *IEEE Trans. Ind. Electron.*, vol. 63, no. 6, pp. 3976–3984, 2016.
[36] D. P. L. Green, "Sperm thrusts and the problem of penetration," *Biol. Rev.*, vol. 63, no. 1, pp. 79–105, 1988.
[37] W. Littmann *et al.*, "Reduction of friction using piezoelectrically excited ultrasonic vibrations," *Proc. SPIE*, vol. 4331, pp. 302–311, 2001.

Authorized licensed use limited to: CITY UNIV OF HONG KONG. Downloaded on February 14,2025 at 08:33:45 UTC from IEEE Xplore. Restrictions apply.